OXFORD CDE

Journal of Computational Design and Engineering, 2021, 8(6), 1562–1575

https://doi.org/10.1093/jcde/qwab061
Journal homepage: www.jcde.org

RESEARCH ARTICLE

Design synthesis and optimization of a 4-SPS intrinsically compliant parallel wrist rehabilitation robotic orthosis

Shahid Hussain [1,*], Prashant K. Jamwal[2] and Paulette Van Vliet[3]

[1]Human-Centred Technology, Research Center, Faculty of Science and Technology, University of Canberra, Bruce, Canberra, ACT 2617, Australia; [2]Department of Electrical and Computer Engineering, Nazarbayev University, Astana 010000, Kazakhstan and [3]Research and Innovation Division, University of Newcastle, Callaghan, NSW 2308, Australia

*Corresponding author. E-mail: shahid.hussain@canberra.edu.au https://orcid.org/0000-0002-4352-0212

Abstract

Neuroplasticity allows the human nervous system to adapt and relearn motor control following stroke. Rehabilitation therapy, which enhances neuroplasticity, can be made more effective if assisted by robotic tools. In this paper, a novel 4-SPS parallel robot has been developed to provide recovery of wrist movements post-stroke. The novel mechanism presented here was inspired by the forearm anatomy and can provide the rotational degrees of freedom required for all wrist movements. The robot design has been discussed in detail along with the necessary constructional, kinematic, and static analyses. The spatial workspace of the robot is estimated considering various dimensional and application-specific constraints besides checking for singular configurations. The wrist robot has been further evaluated using important performance indices such as condition number, actuator forces, and stiffness. The pneumatic artificial muscles exhibit varying stiffness, and therefore, workspace points are reached with different overall stiffness of the robot. It is essential to assess robot workspace points that can be reached with positive forces in actuators while maintaining a positive definite overall stiffness matrix. After the above analysis, design optimization has been carried out using an evolutionary algorithm whereby three critical criteria are optimized simultaneously for optimal wrist robot design.

Keywords: compliant actuation; design optimization; parallel robot; stroke rehabilitation; wrist orthosis

1. Introduction

Robot-aided physical rehabilitation is an active trend for subjects suffering from stroke and incomplete spinal cord injuries (Ben-Tzvi *et al.*, 2016; Hunt *et al.*, 2016; Manna & Dubey, 2019; Li *et al.*, 2020; Wang *et al.*, 2020). The wrist is an important and anatomically complicated joint in the upper limb, and approximately 90% of stroke survivors require wrist rehabilitation (Mozaffarian *et al.*, 2016; Wang *et al.*, 2018). The large population of stroke survivors requiring rehabilitation of wrist joint makes robotic devices an economical choice. These robots can provide repetitive, task-specific, and prolonged training sessions as well as objective measurements as compared to manual physical therapy.

Several robotic devices have been developed and reported in the literature for wrist joint rehabilitation. A detailed review on the design and control aspects of wrist rehabilitation robots has recently been published by Hussain *et al.* (2020). These robotic devices have been categorized into end-effector-based and orthoses (i.e. exoskeleton)-based devices. The

Received: 13 May 2021; **Revised:** 21 August 2021; **Accepted:** 7 September 2021

end-effector-based rehabilitation robots are modified versions of industrial robotic manipulators where the patient holds the end effector with hand and the end effector provides motions in multiple degrees of freedom (dof) of the wrist joint. The natural movements required at the wrist joint are abduction/adduction, flexion/extension, and pronation/supination. A servo motor-powered end-effector-based wrist rehabilitation robot developed at MIT (Krebs *et al.*, 2007) provides three powered dof for abduction/adduction, flexion/extension, and pronation/supination of the wrist joint. Similarly, a DC motor-powered end-effector-based wrist rehabilitation robot has been developed at IIT Genova to provide three active dof (Squeri *et al.*, 2014). Several other end-effector-based wrist rehabilitation robots powered by electromagnetic actuators are reported in the literature, which can provide one (Lum *et al.*, 1993; Hesse *et al.*, 2003; Xu *et al.*, 2019), two (Lambercy *et al.*, 2007, 2011; Akdoğan *et al.*, 2018), or three (Oblak *et al.*, 2010; Khor *et al.*, 2017) dof wrist motions. However, the end-effector-based wrist rehabilitation robots have limitations, as it is difficult to ascertain whether the robot forces are applied accurately over the wrist joint or not. To overcome these limitations, several orthoses-based wrist rehabilitation robots have been designed. These robotic orthoses provide better alignment of robotic orthosis joints with anatomical wrist position. They can therefore apply forces at more appropriate locations to the anatomical wrist as compared with their end-effector-based counterparts. The most notable among robotic wrist orthoses is the DC motor-powered *Ricewrist* that can assess motor functions of subjects suffering from SCI besides providing three dof to the wrist joint (Gupta *et al.*, 2008; Pehlivan *et al.*, 2015; Rose *et al.*, 2018). Various other wrist rehabilitation orthoses worth mentioning here can provide one (Burgar *et al.*, 2000; Ren *et al.*, 2013; Amirabdollahian *et al.*, 2014; Beom *et al.*, 2016; Nam *et al.*, 2017) and two (Rahman *et al.*, 2015; Higuma *et al.*, 2018) dof.

The above-mentioned electromagnetic actuated robotic orthoses have a high end-point impedance, which presents limitations for safe human–robot interactions and the implementation of control algorithms for providing Assist-as-Needed robotic rehabilitation. Compliant actuation of robots is an emerging research field (Vallery *et al.*, 2008; Kim *et al.*, 2016; de Souza & Silva, 2020), and several robotic orthoses powered by compliant actuators have been developed for upper (Cui *et al.*, 2017) and lower limb rehabilitation (Jamwal *et al.*, 2014; Hussain *et al.*, 2017). However, very few attempts have been reported in the literature regarding compliant actuation of wrist rehabilitation robotic orthoses. An end-effector type of wrist rehabilitation orthosis powered by Series Elastic Actuators (SEAs; Veneman *et al.*, 2006) called WRES has recently been developed (Buongiorno *et al.*, 2018). However, there are certain limitations associated with the use of SEA for powering the robotic orthoses, such as higher stiffness, achievable passivity, and extensive instrumentation requirements (Hussain et al., 2013). Recently, pneumatic artificial muscles (PAMs) are being utilized to actuate rehabilitation robots as an alternative to SEA (Jamwal *et al.*, 2015). Bartlett *et al.* at Harvard University proposed a soft orthosis for wrist rehabilitation employing PAMs (Bartlett *et al.*, 2015). The prototype developed at Harvard could achieve the required wrist motions and has also been tested on healthy subjects. However, technical details such as how motions are realized and how actuators are controlled have not been included in the manuscript. The primary design flaw of this design is the direct contact of actuators with the skin, which may be inconvenient and hazardous in the event of actuator rupture.

Hassanin *et al.* have proposed a wrist rehabilitation exoskeleton that is a soft robot. However, it can only provide two dof and cannot generate supination/pronation motions (Al-Fahaam *et al.*, 2016). Another wrist robot (EXOWRIST) actuated using pneumatic air muscles, proposed by Andrikopoulos *et al.*, suffers a similar limitation (Andrikopoulos *et al.*, 2015). It can only provide two dof, namely extension–flexion and ulnar–radial deviation. While PAMs have apparent advantages of being lightweight, powerful, and inherently compliant, they are challenging to model, and control and pose many challenges due to their transient and non-linear behaviour (Hassan *et al.*, 2019; Peng *et al.*, 2019; Yuan *et al.*, 2019). PAMs work with compressed air and therefore, their stiffness also changes non-linearly with change in air pressure (Antonelli *et al.*, 2019; Li *et al.*, 2019; Sun *et al.*, 2019). Further, PAMs can only operate under tension (cannot exert compressive forces), and in such a scenario, it is essential to ascertain that the robot workspace points can be reached with positive forces in actuators while maintaining a positive definite overall stiffness matrix (Zhao & Zi, 2014; Sadati *et al.*, 2017).

From the above discussion, it can be established that a robot-assisted rehabilitation for the wrist joint will be both economical and a time-efficient option for the healthcare providers. Further, out of the two options, namely, a robotic orthosis and an end-effector robot, robotic orthosis should be preferred over the end-effector robot. An orthosis applies forces at the wrist joint quite similar to the forearm muscles and hence better accuracies of force transmission are expected. Furthermore, a robotic orthosis actuated by PAMs should be preferred over those actuated by electrical motors due to the safety concerns and need for a complaint actuation during the rehabilitation process. There are at least three instances of wrist robotic orthoses, proposed in the literature, that are actuated using PMAs (Andrikopoulos *et al.*, 2015; Bartlett *et al.*, 2015; Al-Fahaam *et al.*, 2016). However, they suffer from two critical shortcomings, while some of the designs are unsafe owing to the direct contact of their actuators with the skin of the human forearm, the other designs cannot provide supination/pronation motions.

After carefully studying the wrist and forearm anatomy and the existing orthoses, a novel mechanism for wrist rehabilitation orthosis is conceptualized and developed during the proposed research that can also provide the supination/pronation wrist motions. The proposed mechanism is essentially a parallel robot and is inherently compliant owing to using PAMs as actuators. Parallel robots are preferred over serial robots due to their compact designs and higher stiffness (Li *et al.*, 2009); however, a poor design of parallel robots can also lead to a reduced workspace, dof, and higher force requirements (Brinker *et al.*, 2018; Raoofian *et al.*, 2018; Anvari *et al.*, 2019). Normally, the parallel robot designs are evaluated for their feasibility using kinematic and geometrical analyses. Important performance indices, such as condition number, manipulability, tensionability, etc., are also used to determine the quality of the robot workspace (Brinker *et al.*, 2018; Glorieux *et al.*, 2018; Hu *et al.*, 2020). In this paper, the design of the wrist orthosis has been discussed in detail along with the necessary constructional, kinematic, and static analyses. The spatial workspace of the robot is estimated considering various dimensional and application-specific constraints to avoid the singular configurations. The wrist robot is actuated using PAMs that exhibit varying stiffness, and therefore, the workspace points are reached with different overall stiffness of the robot. It is essential to obtain a set of robot workspace points that can be reached with positive forces in the actuators while the overall stiffness matrix also remains positively

Table 1: Ranges of motion for the human wrist (Neese *et al.*, 1989).

Wrist and forearm motions	Range	Mean	Standard deviation	Moments Nm
Supination/pronation	90^0–60^0/76^0–60^0	74.5^0/68.8^0	11^0/6.2^0	26.01/23.99
Flexion/extension	134^0–154^0	106^0	18^0	8.92/7.15
Radial/ulnar	80^0–71^0/83^0–74^0	75.8^0/79.5^0	3.8^0/3.9^0	29.73/16.22

definite. Robot design optimization has been carried out later, implementing an evolutionary algorithm (EA) to obtain an optimal wrist robot design.

The robot design is discussed in detail along with necessary constructional niceties in Section 2. Kinematic design analysis is described in Section 3, where Robot Jacobian analysis and kinematics are discussed. Later in Section 4, robot design performance indices are discussed and enumerated besides a thorough analysis of spatial workspace. Kinematic design optimization of the proposed wrist robot is described in Section 5, followed by a final overall discussion and suggestions for future work. According to the authors' best knowledge, an intrinsically compliant parallel robotic orthosis for wrist rehabilitation is proposed for the first time.

2. Wrist Robot Construction

At the onset, biomechanics of the wrist joint is discussed to derive various specifications for the wrist robot in terms of its types of trajectories and ranges of motions. Followed by the specifications, details on the wrist robot's construction are being laid out here with niceties of various parts about their functions and importance.

2.1 Wrist biomechanics and robot specifications

The wrist joint is a complex biaxial joint operating with remarkable stability between forearm and hand to provide a wide range of three rotational degrees of motions (Talwalkar *et al.*, 2005). Wrist motions can be independent as well as combined with the forearm motions. Independently, the wrist acts as an ellipsoidal-type synovial joint and allows motions along two axes, such as flexion–extension and adduction–abduction (ulnar–radial deviation). Rotation of the hand, which is also termed as pronation and supination, however, is a combined motion of the wrist with the forearm. All the motions occurring at the wrist are carried out by muscle groups of the forearm.

Yet another significant parameter that influences the design of the wrist rehabilitation robot is the interaction torque experienced during rehabilitation therapy at the wrist–forearm junction. Maximum flexion torque at the wrist can be 11.9 ± 2.9 Nm, while the maximum extension torque is measured as 6.5 ± 1.5 Nm (Yoshii *et al.*, 2015). However, torque requirements about other axes are much lower compared to flexion–extension at the wrist joint (Bandy *et al.*, 2001; Hamilton *et al.*, 2012; Nichols *et al.*, 2013).

The wrist robot should be able to provide three degrees of rotational freedom in a compact workspace. The ranges of these required motions or trajectories along with respective moments are given in Table 1. However, it is important to delineate between the anatomical and functional motion ranges. Zhao *et al.* (2019) have elaborately discussed this issue and have recommended the functional ranges of motions for the wrist joint, which are relatively less than the anatomical ones. According to Zhao *et al.* (2019), functional wrist motions are those that are required during personal care/hygiene activities such as combing hair, fastening shirt buttons, dental care, etc. Experiments involving 40 human subjects and subsequent analysis of the data revealed that all of these tasks could be performed with 60 degrees of extension and 54 degrees of flexion. Further, a 20 degree ulnar deviation together with 17 degrees of radial deviation and a similar range for supination–pronation was sufficient for activities of daily living (Zhao *et al.*, 2019). Apart from the ranges of motion, the wrist robot should also be able to traverse through various prescribed rehabilitation trajectories during training sessions. Important robotic rehabilitation training must include passive training (robot active and user passive), active-assist training (robot cooperates with user), and active range of motion (ROM) training (user active and robot passive), as well as muscle-strengthening training (robot provides a constant resistance or varies the resistance according to the extent of displacement, i.e. acts as an elastic element).

The new wrist robot, proposed in the present research, was designed aiming at the functional motion requirement of the wrist joint. A parallel robot design for the proposed wrist robot was preferred to include the supination/pronation wrist motions, which previous wrist robots (actuated using PAMs) could not provide. However, there are issues with the parallel mechanism-based design and the use of PAM actuators. Parallel mechanisms are good in providing accurate motion within a compact workspace but are subjected to singularity-related issues. A parallel robot design with a condition number close to unity (explained later in Section 4.1) can help in eliminating the singularity issues. Further, since the PMAs are flexible actuators, we need to constantly maintain some nominal pressure inside them, else the robot will collapse. In other words, we need to check the minimum robot stiffness and find ways to maximize it by means of the robot geometrical design. It is possible to alter the robot geometry, which is mainly governed by the placement of the actuators and maximize the minimum overall stiffness. The norm of actuator forces, which is required to achieve target wrist torques, is another important objective. It is desired to achieve the target torques with reduced actuator forces, which is possible by placing the actuators away from the axis of rotation. Therefore, in the present research, first, a wrist robot design is conceptualized, and later through design optimization, the overall minimum stiffness is maximized while the norm of actuator forces is minimized. In the following section, the conceptual design of the new wrist robot is discussed before its kinematic synthesis, which is elaborated in Section 3.

2.2 Conceptual design of wrist parallel robot

Most of the skeletal joints in the human body are actuated by the parallel action of muscle groups. Therefore, a bio-inspired design for wrist robot should be a parallel mechanism. In parallel mechanisms, a movable end effector is linked to a fixed base

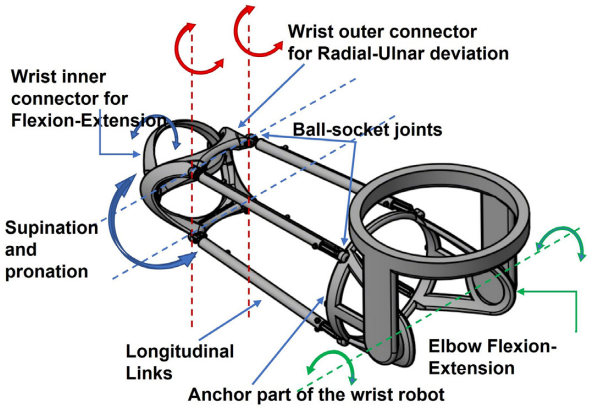

Figure 1: Conceptual design of the robotic orthosis for wrist rehabilitation (ROWR).

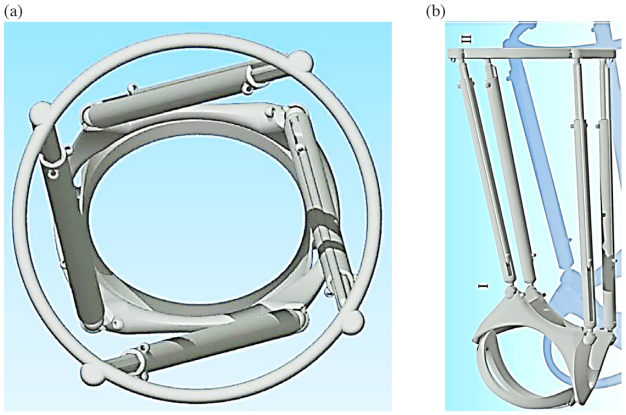

Figure 2: (a) Anchor part (bottom view of Fig. 1) facilitating supination and pronation rotation. (b) Ulnar rotation with the help of four ball–socket joints.

through multiple actuators, and the end effector is manoeuvred by simultaneous motions of parallel configuration of actuators. Owing to this arrangement, the parallel robots do not suffer from accumulated errors that are common in their serial counterparts. Moreover, since the end effector is linked with multiple actuators, its loading capacity, as well as stiffness, is also higher compared to serial robots. In the light of the above discussion, it is evident that a parallel mechanism-based design shall be a more suitable one for the intended wrist robot.

However, parallel robots suffer from the issues of reduced workspace and increased kinematic singularities (Tsai, 1999; Merlet, 2006). The kinematic workspace, here, is defined in terms of the Euler angles (along three axes). A combination of these angles gives an orientation of the robot end effector with respect to the coordinate system, which is assumed to be placed at the anatomical wrist joint shown as 'W' in Fig. 5a and b. Opportunely, since the ROM of the wrist joint is relatively small, the reduced workspace of parallel manipulators may not pose a severe problem provided suitable kinematic variables are selected. On the other hand, singularities offer a much more significant challenge and must be carefully considered while designing the robot. This research therefore places particular attention on the workspace and singularity analyses during the development of the wrist rehabilitation platform.

The distinguishing features of the proposed design are its wearability, expandability, and less intimidating appearance (Fig. 1). While the use of ball and socket joints at both ends of the longitudinal links facilitates rotation of the hand, the expandable longitudinal sections can accommodate a wide range of forearm lengths. The elbow part, at the rear end of this device, is detachable to facilitate the user to don/doff. This simple design, which is compact and straight, appears to be less intimidating compared to previous wrist robots.

In the proposed wrist robot design (Fig. 1), four parallel collapsible longitudinal links with ball–socket joints at both ends (between anchor and wrist outer connector part) are employed. Four PAMs (6 mm diameter and 150 mm long) are attached between the end effector and the anchor part of the robot to provide three dof; one of these is the required supination and pronation motion (Fig. 2a) that is the rotation between the fixed *anchor* (to be fixed on the forearm, Fig. 4) and the moving *end effector* (comprising wrist inner and outer connectors, Fig. 3). Flexion–extension wrist motions together with radial–ulnar deviations (Fig. 2b) are provided by the end-effector part of the wrist robot.

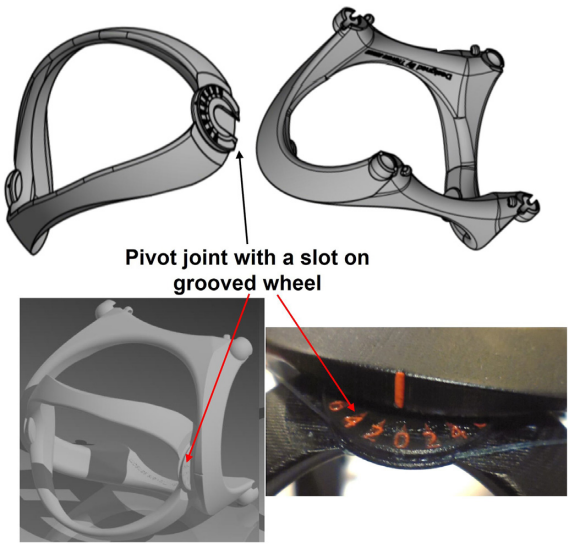

Figure 3: End-effector part of the robot shown with inner and outer parts pivoted together with a slot that allows both parts to slide together.

A wrist inner connector (subject can grip this part rolling over fingers) is joined through two passive revolute joints with the wrist outer part for ease of gripping (Fig. 3). The anchor part (Fig. 4), which helps in wrist rotation about the forearm, is constructed as the initial robot attachment point to the human body using straps at the elbow. Four sockets are also shown in Fig. 4, which are built to house the ball end of four longitudinal links. The sockets are provided with slits for easy fitting and assembly of the ball joints. The wrist robot parts are all fabricated using appropriate tolerances for their required fits.

3. Kinematic Design Analysis

Since the human wrist and forearm will be an integral part of the wrist parallel robot, its kinematic description must be established before further analyses on its workspace, singularities, and moment capabilities.

While anatomically, the wrist joint should be considered as a biaxial joint, in the present research, it is being considered as a spherical joint for convenience without the loss of

Figure 4: Anchor part of the wrist robot to be fitted on the forearm near elbow.

generality. Previous research suggests that orientations of the revolute joints in the wrist biaxial model can vary between subjects (Talwalkar *et al.*, 2005), which may adversely affect the inferences drawn for the workspace and singularity analysis. Moreover, the amount of translation is trivial enough to be discarded, and hence the spherical model for the wrist joint is being assumed here.

For a spherical joint and consequent three rotational dof, three actuators should be sufficient for complete mechanism controllability. However, since the PAMs are flexible actuators and cannot provide a 'push' force, redundant actuation is indispensable. The kinematic configuration considered in this research is shown in Fig. 5a, together with details of the variables used to define actuator connection points and two end platforms (anchor and the end effector) of the proposed parallel robot (Fig. 5b).

While the anchor is to be strapped to the forearm, the wrist connectors need to be adjusted (by altering lengths of longitudinal links) to fit with the hand of the user. The actuator (PAM) connection points at the anchor are all shown by a_i while on the end effector (wrist connector), these are given by b_i. Both a_i and b_i are coincident with the centres of the ball–socket joints at the two ends of longitudinal links. The centre of anchor part O_o is coplanar with a_i points, and since it does not move relatively, it is termed as the origin of the global reference frame. Similarly, O_e, which is the centre of the end effector, is also coplanar with b_i points and is termed as the origin of the end-effector frame. The wrist joint, considering it a ball and socket joint, is assumed to be placed at 'W'.

The robot design parameters mainly consist of the geometrical parameters and the actuator connection points. It is known that the parallel robot's kinematic performance largely depends on its geometrical parameters (Merlet, 2010). By altering these parameters, it is possible to obtain a robot design that provides accurate motions with less force requirements. Radii of actuator connection points at anchor (which is analogous to the base of the parallel robot) and at the end effector are shown as q_2 and q_5, respectively. To begin with, the angular placements of actuators on both the platforms (Fig. 5a, q_1 and q_3 on anchor and q_4 and q_6 on the end effector) are chosen using our previous knowledge about parallel platforms (Jamwal *et al.*, 2015).

For further discussion on kinematic analysis, the end effector is assumed to be pivoted about the centre of the anatomical wrist joint (W). Subsequently, when the forearm is fixed with the anchor platform, and the wrist is placed on the robot end effector, the wrist joint would be completely isolated. Therefore, motion and torques of the end effector about the wrist centre will provide precise values of the relative orientation and torques between the user's hand and forearm.

3.1 Inverse kinematics

Mapping of the end-effector orientations to its corresponding actuator linear displacements is termed as the inverse kinematics (IK) of a parallel robot. While IK for serial robots provides redundant solutions, a singular solution can be obtained for parallel robots (Keemink *et al.*, 2018). This relationship can be devised using the kinematic variables discussed in the previous section. The relaxed length of the actuator can be defined as the one when the end-effector frame is identically aligned with the robot global frame or the anchor frame (home configuration). The length vector of the ith actuated longitudinal link can be written as (1), while the magnitude of its length is given by (2).

$$L_i = \overrightarrow{O_o W} - \overrightarrow{O_o a_i} + R\left(\overrightarrow{W b_{i,0}}\right) \tag{1}$$

$$l_i = \sqrt{L_i^{tr} L_i} \tag{2}$$

Here, subscript '0' represents quantities relating to the home configuration, and R is the rotational transformation matrix of end effector for a stationary axis rotation sequence of ψ, θ, and φ.

3.2 Robot Jacobian analysis

Robot's Jacobian matrix, in general, describes the relationship between the velocities of joint space (longitudinal links) and task space (end effector). With regard to parallel robots, there exists a unique set of link displacement (dl) for a given end-effector orientation (dp), as shown in (3). Alternatively, the robot Jacobian J can be defined as a gradient matrix that maps the end-effector velocity 'ω' to the link velocity 'v' (3). It is interesting to note that the transpose of the Jacobian matrix also maps the link forces to end-effector forces (4). Therefore, robot's Jacobian matrix can provide information on the kinetics and kinematics for a given robot pose/configuration. Since the Jacobian is the gradient matrix, it can be obtained by differentiating (1), and the ith row of robot Jacobian can be given by (5).

$$dl = J\, dp \text{ or } v = J\,\omega \tag{3}$$

$$\boldsymbol{\tau} = J^{tr}\,\mathbf{F} \tag{4}$$

$$J_i = \frac{1}{l_i} L_i{}^{tr} \left[\frac{\partial R}{\partial \psi} b_{i,0} \;\; \frac{\partial R}{\partial \theta} b_{i,0} \;\; \frac{\partial R}{\partial \varphi} b_{i,0} \right] \tag{5}$$

Robot Jacobian plays an important role in identifying possible singular configurations in the robot workspace. Singular configurations in the robot workspace are orientations of the robot where the robot Jacobian becomes rank deficient. In other words, the singular configurations are normally related to a very high

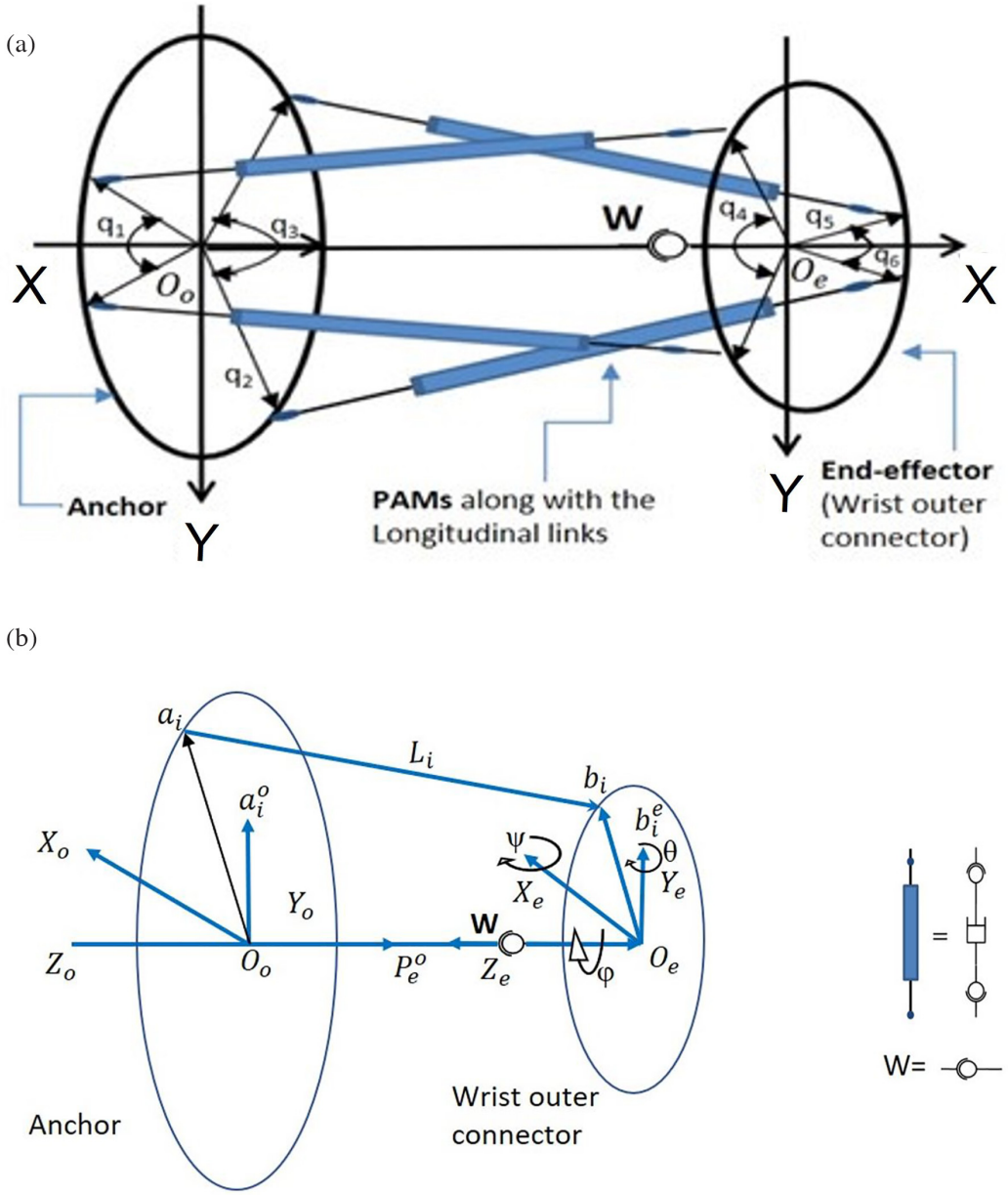

Figure 5: (a) Schematic of the wrist robot. (b) Line sketch of the wrist robot and actuators.

condition number value (or infinite) or zero matrix determinant of the Jacobian matrix (if the manipulator Jacobian is a square matrix). Consequent to the rank deficiency in the Jacobian matrix, the robot shall lose controllability, and regardless of the joint space forces, end-effector forces may not be realized along certain directions. Singular configurations can also be defined as poses where the robot gains additional dof during motion. The presence of null space in the robot Jacobian will result in certain end-effector velocities even if all the actuators are locked (i.e. zero link velocities). Evidently, the selection of robot kinematic variables becomes important to avoid singular configurations from the workspace of the robot. The robot will lose controllability even in the vicinity of singular points, and therefore, a good kinematic design should aim to reduce singular configurations in the robot workspace to improve its manipulability. This can be done by controlling the condition numbers of robot Jacobian in the entire end-effector workspace, as discussed in the following subsection.

4. Design Performance Criteria

It is clear from the discussion in the previous section that the selection of robot kinematic variables is important from the perspective of its kinematic and kinetic performances. Hence, ahead of its detailed design and implementation, robot design should be evaluated on certain performance criteria. To check for the singularity regions in the robot workspace, condition numbers of the Jacobian matrix at various workspace points should be assessed. Since the actuators are flexible and can only provide a pull 'force', it is essential to check whether the workspace points can be reached with positive actuator forces. The set of all such workspace points is termed as the force

Figure 6: First prototype constructed for wrist rehabilitation robot using some redundant actuators.

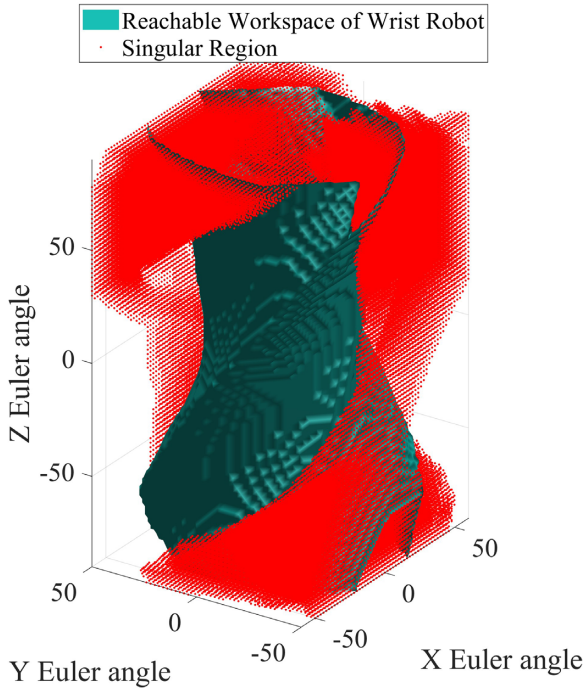

Figure 7: Workspace volume [points $k(J) > 10$ are in red] of the wrist robot is defined with the Euler angles along the three axes. Here, X, Y, and Z Euler angles are for the flexion–extension, supination–pronation, and radial–ulnar, respectively.

feasible workspace (FFW). Robot kinematic variables affect the Jacobian matrix, which in turn maps the link forces and end-effector torques (4). By selecting appropriate kinematic variables, it is possible to enhance the FFW, and at the same time minimize actuator force requirement. The actuators (PAMs) exhibit varying stiffness, and therefore, the robot end effector reaches out various workspace points with different overall stiffness of the robot. It is essential to check whether the overall stiffness matrix is positive definite or not in the entire robot workspace. Workspace points complying with the constraint posed by stiffness criteria are termed as stiffness feasible workspace. The overall reachable workspace of the robot should also comply with the anatomical wrist workspace requirements. The first prototype of the wrist robot constructed at the University of Canberra is shown in Fig. 6. This being the initial fail-safe design, the actuators are arranged in many different fashions (including some redundant ones) to evaluate actuations and orientations.

A brief discussion around various design performance criteria is provided here, besides their mathematical formulations to be used in a design optimization process later.

4.1 Condition number and singularity analysis

The Jacobian matrix of the robot (J) maps its link velocities to its end-effector velocities (3). Jacobian matrix can be evaluated by a performance index called condition number. A condition number (of J matrix) measures how sensitive end-effector velocities are to perturbations in the link velocities and round-off errors. The norm of Jacobian matrix J measures how much the relevant mapping can stretch vectors.

$$M = \|J\| = \max \frac{\|J\,\omega\|}{\|\omega\|} \tag{6}$$

It is also worthwhile to find possible shrinkage a matrix can do:

$$m = \min \frac{\|J\,\omega\|}{\|\omega\|}. \tag{7}$$

Condition number of Jacobian matrix $k(J)$ can be defined as the ratio of the maximum to minimum stretching as given below:

$$k(J) = \frac{M}{m} \quad \text{or} \quad k(J) = \|J\| \,.\, \|J^{-1}\|. \tag{8}$$

Equation (3) can be analysed for perturbations as below:

$$J(\omega + \delta\omega) = v + \delta v. \tag{9}$$

Here, δv denotes the errors in link velocities that cause errors ($\delta\omega$) in the end-effector velocities. The definition of M and m gives us the following:

$$\begin{gathered} \|v\| \le M\|\omega\| \quad \text{and} \quad \|\delta v\| \ge m\|\delta\omega\| \ \text{provided that}\ m \neq 0 \\ \frac{\|\delta\omega\|}{\|\omega\|} \le k(J)\,\frac{\|\delta v\|}{\|v\|}. \end{gathered} \tag{10}$$

Therefore, it is evident that fractional change in the link velocities ($\frac{\|\delta v\|}{\|v\|}$) results in fractional changes in the end-effector velocities ($\frac{\|\delta\omega\|}{\|\omega\|}$). The benefit of using fractional changes is that since they are dimensionless, they are not affected by any scale factor or by the magnitude of errors. Since a low value of condition number (k) can decrease the error in the end-effector velocities and torques (4), it is desired to achieve a near-unity condition number for robot designs (Jamwal & Hussain, 2016) in the entire workspace. Workspace volume from the first prototype is illustrated in Fig. 7, where points with condition number [$k(J)$] greater than 10 are shown in red colour.

The distribution of condition number values in the entire robot workspace is also shown in Fig. 8. Condition number also provides information about the singular configurations. For instance, a singular matrix (J) can result in non-zero end-effector velocities and torques while the link velocities and forces are all zero. Higher values of condition number also indicate that the robot is in the vicinity of singular configuration. Global perspective of condition number, Global Condition Number (GCN),

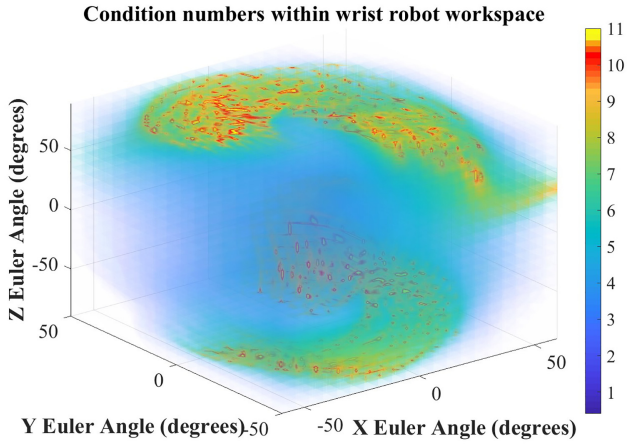

Figure 8: Distribution of condition number in the robot workspace that is defined by the Euler angles through which the wrist robot can traverse along the three cartesian axes.

is much useful since it evaluates robot configurations in its entire workspace (Jamwal *et al.*, 2015).

The mean of '*k*' values, at '*n*' discrete workspace points, is taken as the global measure of the robot condition number. The robot configuration is termed as ill-conditioned if the GCN number is large and is considered well conditioned for near-unity GCN. To obtain optimal robot kinematic variables, the global index of condition number should be minimized. An optimization problem in this context is formulated as below.

$$\text{Minimize } GCN(J) = \frac{\sum_{i=1}^{n} \left(\|J\| . \|J^{-1}\|\right)}{n} \tag{11}$$

4.2 Static force analysis

To realize a given end-effector wrench (τ_e) at the end effector, a set of robot link forces (F) is required (4), which can be calculated using J, and assuming the end effector to be a rigid body (ignoring any deformation). The Jacobian matrix provides linear transformations between link forces and end-effector torques and therefore, it will become singular in the event of a possible coupling between link forces. While in singular configuration, the robot may generate large end-effector torques in response to a small change in the link forces. It is therefore desired that the link forces be linearly independent and not coupled.

From the design optimization perspective, the minimization of the norm of actuator forces and individual maximum actuator force is considered as one of the objectives in this research. The criterion for optimization in this regard is formulated as given by (12).

$$\text{Minimize } F_N = \left\{\text{norm}\left([J^{tr}]^{-1}\tau\right) + \max\left([J^{tr}]^{-1}\tau\right)\right\} \tag{12}$$

4.3 Link forces and stiffness analysis

The static force balance equation for the parallel robot can be written as (13). Here, end-effector wrench (τ) can be obtained as a result of actuator forces (F).

$$J^{tr}F - \tau = 0 \tag{13}$$

Differentiating (13) with respect to end-effector orientation (dp), the stiffness matrix can be derived as (14).

$$S = \frac{d\tau}{dp} = J^{tr}\frac{dF}{dp} + \frac{d}{dp}J^{tr}F = J^{tr}\frac{dF}{dl}\frac{dl}{dp} + \frac{d}{dp}J^{tr}F \tag{14}$$

$$\text{Or} \quad S = \frac{d\tau}{dp} = J^{tr}\,diag(k_1, .., k_4)J + \frac{d}{dp}J^{tr}F \tag{15}$$

Thereby, the overall stiffness is the sum of individual actuator stiffness ($k_1, \ldots, k_4$) besides stiffness due to internal forces introduced because of redundant actuation. As mentioned previously, while using PAMs, redundant actuation is needed to achieve the required dof. The redundant actuation generates internal forces whose resultant torque on the end effector is zero but gives rise to added stiffness shown as the second part in (15).

It is known that a parallel robot employing flexible actuators can be termed as stabilizable provided its overall stiffness matrix remains positive definite (using antagonistic PAMs actuation) under any arbitrary loading (Behzadipour & Khajepour, 2006). The redundant actuation of the wrist robot provides an extra dof in the null space solution of the robot's Jacobian matrix (J). The benefit from this extra dof is that the end effector can be manipulated in the robot's workspace with positive (or tension) forces in the actuators. Therefore, it can be shown that both terms in (15) will be always positive definite. Moreover, owing to the parallel configuration of the wrist robot, the overall stiffness is always higher than the highest individual link stiffness.

The PAMs are connected with cables and therefore have two stiffnesses in series. Nevertheless, the resultant stiffness ($k_1, \ldots, k_4$) should come from the less stiff PAM. The stiffness of individual PAM can be derived as a function of its internal gauge pressure (P_g) as given in equation (16) (Colbrunn *et al.*, 2001).

$$k = \frac{3P_gL}{2\pi n^2} \tag{16}$$

Here, L is the length of PAM, n is used to show number of turns for a single thread, and b is used for its thread angle. Since this is an empirical relation, the actual stiffness values may vary between PAMs. Since the second part of the overall stiffness (15) comes from the pretension in the actuators and is more or less constant, only the first part of (15) is being considered for robot design optimization. Actuator stiffness matrix $[J^{tr}\text{diag}(k_1, \ldots, k_4)J]$ can be resolved using singular value decomposition in order to establish its physical significance.

$$[S]_{3\times3} = [X^T]_{3\times3}\,[\Sigma]_{3\times3}[Y]_{3\times3} \tag{17}$$

In equation (17), X and Y are orthogonal matrices while Σ is a diagonal matrix consisting of three singular values ($\Sigma_1, \Sigma_2, \Sigma_3$). Interestingly, the minimum of these diagonal values is the minimum actuator stiffness. To enhance the overall stiffness of the robot, it is desired to maximize this minimum stiffness value (18).

$$\text{Maximize } S_{min} = \min(\text{diag}(\Sigma_1, \Sigma_2, \Sigma_3)) \tag{18}$$

It is being emphasized here that a robot design can be evaluated using the above-discussed design criteria. While there are many other design criteria to evaluate and validate robot designs, these three criteria are directly linked, to the robot Jacobian matrix and therefore to the robot geometry. In the following section, design optimization of the wrist robot, satisfying various constraints, is discussed.

5. Optimal Design of Wrist Parallel Robot

Wrist robot design variables are symbolically shown in Fig. 5a. It is important to reiterate here that changes in the robot

design variables ($q_1 \ldots . q_6$) reflect in the Jacobian matrix, which in turn affects robot design performances. Therefore, it is possible to optimize design performance criteria in order to obtain a robot design with higher overall stiffness, minimum actuator force requirement, and a GCN that is close to unity.

As mentioned in Section 3, the constraints on the wrist robot design variables are decided from the author's previous experience with parallel robot design (Jamwal *et al.*, 2015). The multicriteria optimization problem can be defined as below:

$$\begin{aligned}
&\text{Minimize} \quad \text{GCN}(J) = \frac{\sum_{i=1}^{n}\left(\|J\|.\|J^{-1}\|\right)}{n}\\
&\text{Minimize} \quad \text{norm}\left\{\left([J^{tr}]^{-1}\tau\right) + \max\left([J^{tr}]^{-1}\tau\right)\right\}\\
&\text{Maximize} \quad S_{\min} = \min\left(\text{diag}\left(\Sigma_1, \Sigma_2, \Sigma_3\right)\right)\\
&\text{Subjected to} \quad 0 \le q_1 \text{ and } q_6 \le 120^0\\
&\qquad\qquad 30 \le q_3 \text{ and } q_4 \le 120^0\\
&120\,\text{mm} > |q_2| > 0;\ 100\,\text{mm} > |q_5| > 0.
\end{aligned}$$

To obtain an optimal wrist robot design, three performance criteria, namely global condition number, norm of actuator forces, and robot overall stiffness, are formulated mathematically (11, 12, and 18) in the previous section. Later, it is desired to optimize all of the three criteria simultaneously and obtain an optimal wrist robot design. While dealing with multiple criteria that are interdependent, a preferred approach is to obtain a non-singular set of equitable solutions. A wider set of equitable solutions comprising all possible combinations of trade-offs between objectives provides more visibility in the design process. However, using classical optimization approaches, such a process can be very cumbersome. On the other hand, EAs can handle multiple criteria simultaneously and are able to provide equitable solutions quickly in few iterations (Jamwal *et al.*, 2019). This is possible since EAs work with a large and diverse population of solutions and also apply genetic operators to drive solutions towards evolution to become improved Pareto solutions. Apart from many existing EAs, Non-dominated Sorting Genetic Algorithm-II (NSGA-II; Deb *et al.*, 2002) and Strength Pareto Evolutionary Algorithm 2 (SPEA-2; Kim *et al.*, 2004) have been mostly used in the literature. In the present research, SPEA-2, owing to its benefits over NSGA II, mentioned in Onaka *et al.* (2016), has been adapted to the wrist robot design optimization problem.

5.1 Multicriteria design optimization

SPEA has exhibited remarkable performance in comparison to other multicriteria optimization routines, and the same SPEA now, after certain improvements, is termed as SPEA-2 (Kim *et al.*, 2004). Various steps followed in the algorithmic framework of SPEA-2 are laid down here with a brief explanation.

Step 1: Define an input population (N), an archive set ($\tilde{N}$), maximum number of generations (n), and an output set of non-dominated points (N^D).

Step 2: *Generate* an initial population (P_0) and an empty archive ($Q_0 = \emptyset$); Set $i = 0$.

Step 3: *Assign* strength values (S_i) after calculating fitness of candidate solutions in P_i and Q_i.

$$S(i) = \left|\, j \,|\, j \in (P_i + Q_i) \wedge i \succ j \,\right|$$

Here, $+$ is for union of multiple sets, $\succ$ is used for Pareto dominance, and $i,\ j \in (P_i + Q_i)$. Raw fitness of the candidate solutions is calculated, and non-dominated solutions obtained which with equal raw fitness.

Step 4: *Selection of environment*: Place copies of non-dominated individuals in P_i and Q_i to Q_{i+1}. Use truncation operator if the size of Q_{i+1} exceeds $\tilde{N}$, else fill Q_{i+1} with dominated individuals in P_i and Q_i.

Step 5: *Terminate*. If $i = n$, set N^D as the set of non-dominated individuals in Q_{i+1}, else proceed to Step 6.

Step 6: *Mating selection:* In order to fill the mating pool, perform binary tournament selection with replacements on Q_{i+1}.

Step 7: *Variation:* Obtain resulting population P_{i+1} by applying crossover and mutation operators to the mating pool. Increment generation counter ($i = i + 1$) and go to fitness assignment to reiterate the algorithm.

To begin with, an initial population is generated together with the assignment of an empty archive. The initial population had 500 wrist robot design solutions that were all coded in a binary form. There are six design parameters ($q_1 \ldots q_6$) that are shown in Fig. 5 and also explained in Section 2. These six parameters, together with other known parameters, make up for a wrist robot design. The initial population consists of 500 binary coded strings of 72 bits, each generated using Knuth's random number generator (Knuth, 2000). The binary string of 72 bits has 12 bits assigned for each of the six parameters to discretize the solution space with an accuracy of the order of 10^{-4}. The maximum number of generations (n) was initially set to 1000, and a null archive set ($\tilde{N}$) was defined together with an output set of non-dominated points (N^D). Individuals are selected and sorted based on their fitness evaluation, whereby the three objective function values for each of the robot designs are calculated, and the non-dominated design solutions are selected and stored. If the collective number of non-dominated solutions from the initial population and the archive set is more than 500, the truncation operator is used and if the collective number is less, the empty spaces are filled with the dominated solutions to make the number of solutions as 500. Binary tournament selection with replacements was carried out to fill the mating pool from the two population sets. Genetic operators (crossover and mutation) are applied to the solutions in the mating pool to obtain evolved solutions (Liang *et al.*, 2015). Suitable parametric values while carrying out optimization using SPEA-2 are selected. The crossover probability is kept moderate at 0.7 to avoid a possible blind search otherwise, while the mutation probability is defined as the inverse of the total number of variables. The distribution index for the simulated binary crossover operator and for polynomial mutation is selected to be 15. During the entire run of the SPEA-2 algorithm, an equal proportion of internal

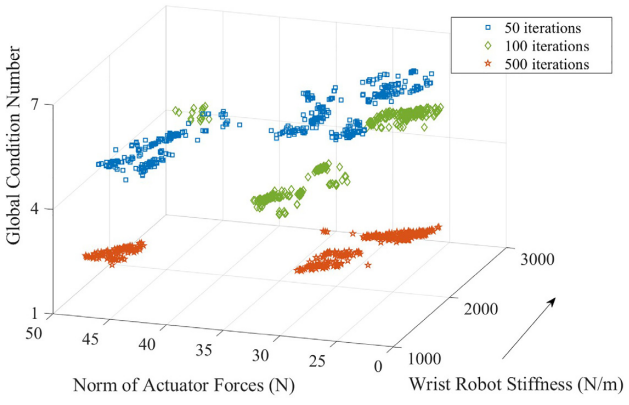

Figure 9: Pareto optimal performances of the wrist robot design solutions against three design criteria after 50 iterations (blue markers), 100 (green markers), and 500 (red markers).

population size to archive size is maintained. Input population (N) of 500 individuals is evolved through the implementation of the SPEA-2 algorithm, and solution populations after 50, 100, and 500 simulation runs were retrieved, and plotted (Fig. 9). The algorithm stopped to converge after 500 iterations.

6. Results and Discussion

After the evolutionary optimization, a set of pareto optimal designs was obtained. The SPEA algorithm was for three times, and each of the times the design solutions stopped evolving after close to 500 iterations. The resulting solution population from the third experiment is taken as the Pareto front solutions. The evolution process is illustrated in Fig. 9, where solutions after three stages of iterations are shown to be improving. While non-dominated solutions in the final population (shown with red markers in Fig. 9) are all equitable, these solutions give different values for the three design criteria. Therefore, it is required to perform an intuitive check while selecting a singular solution from the Pareto set. A wrist robot design solution is finally selected that provides a good trade-off between the design criteria. Design variables of the optimal design (referring to Fig. 5a), after rounding to nearest integers, are as follows:

q_1	q_2	q_3	q_4	q_5	q_6
90^0	120 mm	130^0	130^0	85 mm	90^0

The final robot design was further evaluated for the individual performance metrics. To begin with, the condition number distribution in the robot workspace was evaluated, and it was found to be more than 10 only at the extremities of the workspace and less than 10 at all other points inside the functional workspace (Fig. 8). The global value of the condition number averaged over the entire workspace, however, was found to be 3.25. A condition number of 10 or less is normally accepted to avoid singularity in the parallel robots' workspaces (He *et al.*, 2020; Hoshyarmanesh *et al.*, 2021). The maximum norm of the four actuator forces is found to be 32 N that is slightly less than the maximum force a single actuator can provide. Therefore, the maximum norm from the optimal design remains within the safe actuation limits. The minimum overall stiffness of the optimal robot design (S) is found to be 1700 N/m. The lower limit of stiffness corresponds to the unactuated state, and the upper limit of stiffness, when the robot traverses through the mean of the trajectories, was obtained as 3500 N/m.

The optimal design parameters, thus obtained, were used while developing the laboratory prototype of the wrist robot. It was found that the wrist robot can provide the required functional supination/pronation wrist motions, which is evident from Figs 7 and 8. However, there are certain limitations in this design that will become the basis for the future work. First, the extent of flexion–extension motion from the robot is bit less than the functional ROM of the wrist joint (as seen in Fig. 7). This limitation is solely due to the inadequate actuation from the PAMs and in the future we shall strive to amplify the PAM actuation. The achievable functional workspace of the robot, however, is free from the singularities and owing to the redundant actuation, it can be reached with positive forces (pull force) in the actuators. The overall stiffness matrix of the robot was found to be positively definite in the functional workspace (Fig. 9).

7. Conclusion

Prior to the conceptual design, the anatomy of the human wrist was studied and specifications for a wrist robot were derived. Subsequently, a novel wrist robot design is conceptualized, which is wearable, is inherently compliant, and is based on a parallel mechanism. The proposed design is adaptable to different users, and at the same time is wearable with a friendly appearance (unlike existing robots that have less acceptance from users due to their intimidating structures). To obtain required wrist motions and moments from this robot in a safe manner, it is desired that the design should be evaluated appropriately. Therefore, three important design performance criteria were identified and discussed before formulating mathematically.

Global condition number for the robot is considered important from the perspective of accuracies in wrist motions and torques besides avoiding singular designs. Force analysis is important given the fact that the actuators are flexible and can only apply a pulling force. Using an extra actuator leads to redundancy but at the same time provides an extra dof in the null space solution of the robot's Jacobian matrix (J). This extra dof makes it possible to manoeuvre the robot end effector in the entire reachable workspace with all positive actuator forces. Moreover, since it is possible to minimize actuator forces by altering robot design, the norm of actuator forces (besides maximum actuator force) is selected as one of the design criteria to optimize. While using flexible PAMs, the overall stiffness of the robot poses a big concern, and therefore, the stiffness analysis is carried out considering PAMs in series with cables. Besides ensuring the positive definiteness of the overall stiffness matrix (S), it is also desired to maximize 'S' by means of design changes. The third design criterion therefore is chosen as the maximization of the minimum actuator stiffness. A popular and established multicriteria optimization algorithm, SPEA-2, is implemented for wrist robot design optimization with three design criteria.

In the future course of this research, the prototype shall be constructed as per the optimal design discussed in this manuscript. Trials with human subjects shall be carried out for further evaluation of design with subjects. An appropriate controller shall be designed, implemented, and validated for various wrist rehabilitation procedures.

Acknowledgements

This work was supported by FDCR Grant Program (Ref#021220FD0251). This work was also supported in part by the Seed Grant from the Faculty of Science and Technology, University of Canberra, Canberra, Australia.

Conflict of interest statement

None declared.

References

Akdoğan, E., Aktan, M. E., Koru, A. T., Selçuk Arslan, M., Atlıhan, M., & Kuran, B. (2018). Hybrid impedance control of a robot manipulator for wrist and forearm rehabilitation: Performance analysis and clinical results. *Mechatronics*, 49, 77–91.

Al-Fahaam, H., Davis, S., & Nefti-Meziani, S. (2016). Wrist rehabilitation exoskeleton robot based on pneumatic soft

actuators. In *2016 International Conference for Students on Applied Engineering (ICSAE)*(pp. 491–496).

Amirabdollahian, F., Ates, S., Basteris, A., Cesario, A., Buurke, J., Hermens, H., Hermens, H., Hofs, D., Johansson, E., Mountain, G., Nasr, N., Nijenhuis, S., Prange, G., Rahman, N., Sale, P., Schätzlein, F., van Schooten, B., & Stienen, A. (2014). Design, development and deployment of a hand/wrist exoskeleton for home-based rehabilitation after stroke – SCRIPT project. *Robotica*, *32*, 1331–1346.

Andrikopoulos, G., Nikolakopoulos, G., & Manesis, S. (2015). Motion control of a novel robotic wrist exoskeleton via pneumatic muscle actuators. In *2015 IEEE 20th Conference on Emerging Technologies & Factory Automation (ETFA)*(pp. 1–8).

Antonelli, M. G., Zobel, P. B., Durante, F., & Raparelli, T. (2019). Additive manufacturing applications on flexible actuators for active orthoses and medical devices. *Journal of Healthcare Engineering*, *2019*, 1–11.

Anvari, Z., Ataei, P., & Masouleh, M. T (2019). Collision-free workspace and kinetostatic performances of a 4-DOF delta parallel robot. *Journal of the Brazilian Society of Mechanical Sciences and Engineering*, *41*, 1–7.

Bandy, W., Reese, N., & Bandy, W. (2001). *Joint range of motion and muscle length testing*. Elsevier.

Bartlett, N. W., Lyau, V., Raiford, W. A., Holland, D., Gafford, J. B., Ellis, T. D., & Walsh, C. J. (2015). A soft robotic orthosis for wrist rehabilitation. *Journal of Medical Devices, Transactions of the ASME*, *9*, 1–3.

Behzadipour, S., & Khajepour, A. (2006). Stiffness of cable-based parallel manipulators with application to stability analysis. *Journal of Mechanical Design, Transactions of the ASME*, *128*, 303–310.

Ben-Tzvi, P., Danoff, J., & Ma, Z. (2016). The design evolution of a sensing and force-feedback exoskeleton robotic glove for hand rehabilitation application. *Journal of Mechanisms and Robotics*, *8*, 1–9.

Beom, J., Koh, S., Nam, H. S., Kim, W., Kim, Y., Seo, H. G., Oh, B. M., Chung, S. G., & Kim, S. (2016). Robotic mirror therapy system for functional recovery of hemiplegic arms. *Journal of Visualized Experiments*, *2016*.

Brinker, J., Corves, B., & Takeda, Y. (2018). Kinematic performance evaluation of high-speed Delta parallel robots based on motion/force transmission indices. *Mechanism and Machine Theory*, *125*, 111–125.

Buongiorno, D., Sotgiu, E., Leonardis, D., Marcheschi, S., Solazzi, M., & Frisoli, A. (2018). WRES: A novel 3 DoF WRist ExoSkeleton with tendon-driven differential transmission for neuro-rehabilitation and teleoperation. *IEEE Robotics and Automation Letters*, *3*, 2152–2159.

Burgar, C. G., Lum, P. S., Shor, P. C., & Van Der Loos, H. F. M. (2000). Development of robots for rehabilitation therapy: The Palo Alto VA/Stanford experience. *Journal of Rehabilitation Research and Development*, *37*, 663–673.

Colbrunn, R. W., Nelson, G. M., & Quinn, R. D. (2001). Modeling of braided pneumatic actuators for robotic control. In *Proceedings of the International Conference on Intelligent Robots and Systems*.

Cui, X., Chen, W., Jin, X., & Agrawal, S. K. (2017). Design of a 7-DOF Cable-Driven Arm Exoskeleton (CAREX-7) and a controller for dexterous motion training or assistance. *IEEE/ASME Transactions on Mechatronics*, *22*, 161–172.

de Souza, E. M., & Silva, E. C. N. (2020). Topology optimization applied to the design of actuators driven by pressure loads. *Structural and Multidisciplinary Optimization*, *61*, 1763–1786.

Deb, K., Pratap, A., Agarwal, S., & Meyarivan, T. (2002). A fast and elitist multiobjective genetic algorithm: NSGA-II. *IEEE Transactions on Evolutionary Computation*, *6*, 182–197.

Glorieux, E., Franciosa, P., & Ceglarek, D. (2018). End-effector design optimisation and multi-robot motion planning for handling compliant parts. *Structural and Multidisciplinary Optimization*, *57*, 1377–1390.

Gupta, A., O'Malley, M. K., Patoglu, V., & Burgar, C. (2008). Design, control and performance of RiceWrist: A force feedback wrist exoskeleton for rehabilitation and training. *International Journal of Robotics Research*, *27*, 233–251.

Hamilton, N., Weimar, W., & Luttgens, K. (2012). *Kinesiology: Scientific basis of human motion*(p. c2012). McGraw-Hill.

Hassan, T., Cianchetti, M., Moatamedi, M., Mazzolai, B., Laschi, C., & Dario, P. (2019). Finite-element modeling and design of a pneumatic braided muscle actuator with multifunctional capabilities. *IEEE/ASME Transactions on Mechatronics*, *24*, 109–119.

He, P., Xu, B., & Kang, J. (2020). Spherical parallel instrument for daily living emulation (SPINDLE) to restore motor function of stroke survivors. In *Proceedings of the IEEE RAS and EMBS International Conference on Biomedical Robotics and Biomechatronics*(pp. 364–369).

Hesse, S., Schulte-Tigges, G., Konrad, M., Bardeleben, A., & Werner, C. (2003). Robot-assisted arm trainer for the passive and active practice of bilateral forearm and wrist movements in hemiparetic subjects. *Archives of Physical Medicine and Rehabilitation*, *84*, 915–920.

Higuma, T., Kiguchi, K., & Arata, J. (2018). Low-profile two-degree-of-freedom wrist exoskeleton device using multiple spring blades. *IEEE Robotics and Automation Letters*, *3*, 305–311.

Hoshyarmanesh, H., Zareinia, K., Lama, S., & Sutherland, G. R. (2021). Structural design of a microsurgery-specific haptic device: NeuroArmPLUSHD prototype. *Mechatronics*, *73*, In press: https://doi.org/10.1016/j.mechatronics.2020.102481.

Hu, M., Wang, H., & Pan, X. (2020). Multi-objective global optimum design of collaborative robots. *Structural and Multidisciplinary Optimization*, *62*, 1547–1561.

Hunt, J., Lee, H., & Artemiadis, P. (2016). A novel shoulder exoskeleton robot using parallel actuation and a passive slip interface. *Journal of Mechanisms and Robotics*, *9*, 1–7.

Hussain, S., Jamwal, P. K., Ghayesh, M. H., & Xie, S. Q. (2017). Assist-as-needed control of an intrinsically compliant robotic gait training orthosis. *IEEE Transactions on Industrial Electronics*, *64*, 1675–1685.

Hussain, S., Jamwal, P. K., Vliet, P. V., & Ghayesh, M. H. (2020). State-of-the-art robotic devices for wrist rehabilitation: design and control aspects. *IEEE Transactions on Human-Machine Systems*, *50*, 361–372.

Hussain, S., Xie, S. Q., & Jamwal, P. K. (2013). Robust nonlinear control of an intrinsically compliant robotic gait training orthosis. *IEEE Transactions on Systems, Man, and Cybernetics: Systems*, *43*, 655–665.

Jamwal, P. K., Xie, S. Q., Hussain, S., & Parsons, J. (2014). An adaptive wearable parallel robot for the treatment of ankle injuries. *IEEE/ASME Transactions on Mechatronics*, *19*, 64–75.

Jamwal, P. K., Hussain, S., & Xie, S. Q. (2015). Three-stage design analysis and multicriteria optimization of a parallel ankle rehabilitation robot using genetic algorithm. *IEEE Transactions on Automation Science and Engineering*, *12*, 1433–1446.

Jamwal, P. K., & Hussain, S. (2016). Multicriteria design optimization of a parallel ankle rehabilitation robot: Fuzzy

dominated sorting evolutionary algorithm approach. *IEEE Transactions on Systems, Man, and Cybernetics: Systems*, *46*, 589–597.

Jamwal, P. K., Abdikenov, B., & Hussain, S. (2019). Evolutionary optimization using equitable fuzzy sorting genetic algorithm (EFSGA). *IEEE Access*, *7*, 8111–8126.

Keemink, A. Q. L., Van Oort, G., Wessels, M., & Stienen, A. H. A. (2018). Differential inverse kinematics of a redundant 4r exoskeleton shoulder joint. *IEEE Transactions on Neural Systems and Rehabilitation Engineering*, *26*, 817–829.

Khor, K. X., Chin, P. J. H., Yeong, C. F., Su, E. L. M., Narayanan, A. L. T., Abdul Rahman, H., Abdul Rahman, H., & Khan, Q I. (2017). Portable and reconfigurable wrist robot improves hand function for post-stroke subjects. *IEEE Transactions on Neural Systems and Rehabilitation Engineering*, *25*, 1864–1873.

Kim, M., Hiroyasu, T., Miki, M., & Watanabe, S. (2004). SPEA2+: Improving the performance of the strength pareto evolutionary algorithm 2. In *Lecture Notes in Computer Science (including subseries Lecture Notes in Artificial Intelligence and Lecture Notes in Bioinformatics)*(Vol. *3242*, pp. 742–751).

Kim, B. J., Yun, D. K., Lee, S. H., & Jang, G. W. (2016). Topology optimization of industrial robots for system-level stiffness maximization by using part-level metamodels. *Structural and Multidisciplinary Optimization*, 54, 1061–1071.

Knuth, D. E. (2000). *The art of computer programming*(Vol. *02*).

Krebs, H. I., Volpe, B. T., Williams, D., Celestino, J., Charles, S. K., Lynch, D., & Hogan, N. (2007). Robot-aided neurorehabilitation: A robot for wrist rehabilitation. *IEEE Transactions on Neural Systems and Rehabilitation Engineering*, *15*, 327–335.

Lambercy, O., Dovat, L., Gassert, R., Burdet, E., Teo, C. L., & Milner, T. (2007). A haptic knob for rehabilitation of hand function. *IEEE Transactions on Neural Systems and Rehabilitation Engineering*, *15*, 356–366.

Lambercy, O., Dovat, L., Yun, H., Wee, S. K., Kuah, C. W., Chua, K. S., Gassert, R., Milner, T. E., Teo, C. L., & Burdet, E. (2011). Effects of a robot-assisted training of grasp and pronation/supination in chronic stroke: A pilot study. *Journal of NeuroEngineering and Rehabilitation*, *8*, 1–12.

Li, H., Yang, Z., & Huang, T. (2009). Dynamics and elastodynamics optimization of a 2-DOF planar parallel pick-and-place robot with flexible links. *Structural and Multidisciplinary Optimization*, *38*, 195–204.

Li, K., Jiang, H., & Cui, Z. (2019). Design for solving negative stiffness problem of redundant planar rotational parallel mechanisms. *International Journal of Robotics and Automation*, *34*, 78–83.

Li, Z., Ren, Z., Zhao, K., Deng, C., & Feng, Y. (2020). Human-cooperative control design of a walking exoskeleton for body weight support. *IEEE Transactions on Industrial Informatics*, *16*, 2985–2996.

Liang, Z., Song, R., Lin, Q., Du, Z., Chen, J., Ming, Z., & Yu, J. (2015). A double-module immune algorithm for multi-objective optimization problems. *Applied Soft Computing Journal*, *35*, 161–174.

Lum, P. S., Reinkensmeyer, D. J., & Lehman, S. L. (1993). Robotic assist devices for bimanual physical therapy: Preliminary experiments. *IEEE Transactions on Rehabilitation Engineering*, *1*, 185–191.

Manna, S. K., & Dubey, V. N. (2019). A portable elbow exoskeleton for three stages of rehabilitation. *Journal of Mechanisms and Robotics*, *11*, 1–10.

Merlet, J. P. (2010). *Parallel robots*. Springer Publishing Company.

Merlet, J.-P. (2006). *Parallel robots*. (2nd ed.). Springer.

Mozaffarian, D., Benjamin, E. J., Go, A. S., Arnett, D. K., Blaha, M. J., Cushman, M., Das, S. R., de Ferranti, S., Després, J. P., Fullerton, H. J., Howard, V. J., Huffman, M. D., Isasi, C. R., Jiménez, M. C., Judd, S. E., Kissela, B. M., Lichtman, J. H., Lisabeth, L. D., Liu, S., Mackey, R. H. et al. (2016). Heart disease and stroke statistics-2016 update a report from the American Heart Association. *Circulation*, *133*, e38–e48.

Nam, H. S., Koh, S., Kim, Y. J., Beom, J., Lee, W. H., Lee, S. U., & Kim, S. (2017). Biomechanical reactions of exoskeleton neurorehabilitation robots in spastic elbows and wrists. *IEEE Transactions on Neural Systems and Rehabilitation Engineering*, *25*, 2196–2203.

Neese, R. M., Konz, S., & Reams, M. (1989). Ranges of motion in the human wrist. In *Proceedings of the Human Factors Society Annual Meeting*(pp. 698–702).

Nichols, J. A., Bednar, M. S., & Murray, W. M. (2013). Orientations of wrist axes of rotation influence torque required to hold the hand against gravity: A simulation study of the nonimpaired and surgically salvaged wrist. *Journal of Biomechanics*, *46*, 192–196.

Oblak, J., Cikajlo, I., & Matjačić, Z. (2010). Universal haptic drive: A robot for arm and wrist rehabilitation. *IEEE Transactions on Neural Systems and Rehabilitation Engineering*, *18*, 293–302.

Onaka, J. H. D., Lima, Á. S. d., Kataoka, V. d. S., Bezerra, U. H., Tostes, M. E. d. L., Vieira, J. P. A., & Vieira, J. (2016). Comparing NSGA-II and SPEA2 metaheuristics in solving the problem of optimal capacitor banks placement and sizing in distribution grids considering harmonic distortion restrictions. In *2016 17th International Conference on Harmonics and Quality of Power (ICHQP)*(pp. 77–82).

Pehlivan, A. U., Sergi, F., & Omalley, M. K. (2015). A subject-adaptive controller for wrist robotic rehabilitation. *IEEE/ASME Transactions on Mechatronics*, *20*, 1338–1350.

Peng, Y., Liu, Y., Yang, Y., Liu, N., Sun, Y., Liu, Y., Yuanyuan, L., Pu, H., Xie, S., & Luo, J. (2019). Development of continuum manipulator actuated by thin McKibben pneumatic artificial muscle. *Mechatronics*, *60*, 56–65.

Rahman, M. H., Rahman, M. J., Cristobal, O. L., Saad, M., Kenné, J. P., & Archambault, P. S. (2015). Development of a whole arm wearable robotic exoskeleton for rehabilitation and to assist upper limb movements. *Robotica*, *33*, 19–39.

Raoofian, A., Taghvaeipour, A., & Ali Kamali, E. (2018). On the stiffness analysis of robotic manipulators and calculation of stiffness indices. *Mechanism and Machine Theory*, *130*, 382–402.

Ren, Y., Kang, S. H., Park, H. S., Wu, Y. N., & Zhang, L. Q. (2013). Developing a multi-joint upper limb exoskeleton robot for diagnosis, therapy, and outcome evaluation in neurorehabilitation. *IEEE Transactions on Neural Systems and Rehabilitation Engineering*, *21*, 490–499.

Rose, C. G., Pezent, E., Kann, C. K., Deshpande, A. D., & O'Malley, M. K. (2018). Assessing wrist movement with robotic devices. *IEEE Transactions on Neural Systems and Rehabilitation Engineering*, *26*, 1585–1595.

Sadati, S. M. H., Naghibi, S. E., Shiva, A., Noh, Y., Gupta, A., Walker, I. D., Althoefer, K., & Nanayakkara, T. (2017). A geometry deformation model for braided continuum manipulators. *Frontiers Robotics AI*, *4*, 1–25.

Squeri, V., Masia, L., Giannoni, P., Sandini, G., & Morasso, P. (2014). Wrist rehabilitation in chronic stroke patients by means of adaptive, progressive robot-aided therapy. *IEEE Transactions on Neural Systems and Rehabilitation Engineering*, *22*, 312–325.

Sun, C., Chen, L., Liu, J., Dai, J. S., & Kang, R. (2019). A hybrid continuum robot based on pneumatic muscles with embedded

elastic rods. In *Proceedings of the Institution of Mechanical Engineers, Part C: Journal of Mechanical Engineering Science*.

Talwalkar, S. C., Hayton, M. J., Trail, I. A., & Stanley, J. K. (2005). Management of the failed biaxial wrist replacement. *Journal of Hand Surgery*, *30*, 248–251.

Tsai, L.-W. (1999). *Robot analysis: The mechanics of serial and parallel manipulators*. John Wiley & Sons.

Vallery, H., Veneman, J., van Asseldonk, E., Ekkelenkamp, R., Buss, M., & van Der Kooij, H. (2008). Compliant actuation of rehabilitation robots. *IEEE Robotics and Automation Magazine*, *15*, 60–69.

Veneman, J. F., Ekkelenkamp, R., Kruidhof, R., Van Der Helm, F. C. T., & Van Der Kooij, H. (2006). A series elastic- and bowden-cable-based actuation system for use as torque actuator in exoskeleton-type robots. *International Journal of Robotics Research*, *25*, 261–281.

Wang, J., Liu, Z., & Fei, Y. (2018). Design and testing of a soft rehabilitation glove integrating finger and wrist function. *Journal of Mechanisms and Robotics*, *11*, 1–14.

Wang, W., Chen, J., Ji, Y., Jin, W., Liu, J., & Zhang, J. (2020). Evaluation of lower leg muscle activities during human walking assisted by an ankle exoskeleton. *IEEE Transactions on Industrial Informatics*, *16*, 7168–7176.

Xu, D., Zhang, M., Xu, H., Fu, J., Li, X., & Xie, S. Q. (2019). Interactive compliance control of a Wrist Rehabilitation Device (WReD) with enhanced training safety. *Journal of Healthcare Engineering*, *2019*, 1–11.

Yoshii, Y., Yuine, H., Kazuki, O., Tung, W. L., & Ishii, T. (2015). Measurement of wrist flexion and extension torques in different forearm positions. *BioMedical Engineering Online*, *14*, 1–10.

Yuan, Y., Yu, Y., & Guo, L. (2019). Nonlinear active disturbance rejection control for the pneumatic muscle actuators with discrete-time measurements. *IEEE Transactions on Industrial Electronics*, *66*, 2044–2053.

Zhao, X., & Zi, B. (2014). Design and analysis of a pneumatic muscle driven parallel mechanism for imitating human pelvis. *Proceedings of the Institution of Mechanical Engineers, Part C: Journal of Mechanical Engineering Science*, *228*, 723–741.

Zhao, K. D., Robinson, C. A., & Hilliard, M. J. (2019). 11 - Biomechanics of the upper limb. In J. B. Webster, & D. P. Murphy (Eds.), *Atlas of orthoses and assistive devices. (5th ed.)*. (pp. 127–133). Elsevier.